# GVHD after haploidentical transplantation: a novel, MHC-defined rhesus macaque model identifies CD28$^-$ CD8$^+$ T cells as a reservoir of breakthrough T-cell proliferation during costimulation blockade and sirolimus-based immunosuppression

*Weston P. Miller,[1,2] *Swetha Srinivasan,[3] Angela Panoskaltsis-Mortari,[2] Karnail Singh,[3] Sharon Sen,[3] Kelly Hamby,[3] Taylor Deane,[3] Linda Stempora,[3] Jonathan Beus,[3] Alexa Turner,[3] Caleb Wheeler,[1] Daniel C. Anderson,[4] Prachi Sharma,[4] Anapatricia Garcia,[4] Elizabeth Strobert,[4] Eric Elder,[5] Ian Crocker,[5] Timothy Crenshaw,[5] M. Cecilia T. Penedo,[6] Thea Ward,[6] Mingqing Song,[3] John Horan,[1] Christian P. Larsen,[3] Bruce R. Blazar,[2] and Leslie S. Kean[1,3]

[1]Aflac Cancer Center and Blood Disorders Service, Children's Healthcare of Atlanta, and Department of Pediatrics, Emory University School of Medicine, Atlanta, GA; [2]Department of Pediatric Hematology-Oncology, University of Minnesota, Minneapolis, MN; [3]The Emory Transplant Center, Department of Surgery, Emory University School of Medicine, Atlanta, GA; [4]The Yerkes National Primate Research Center, Emory University, Atlanta, GA; [5]Department of Radiation Oncology, Winship Cancer Institute, Emory University School of Medicine, Atlanta, GA; and [6]Veterinary Genetics Laboratory, University of California, Davis, Davis, CA

**We have developed a major histocompatibility complex–defined primate model of graft-versus-host disease (GVHD) and have determined the effect that CD28/CD40-directed costimulation blockade and sirolimus have on this disease. Severe GVHD developed after haploidentical transplantation without prophylaxis, characterized by rapid clinical decline and widespread T-cell infiltration and organ damage. Mechanistic analysis showed activation and possible counterregulation, with rapid T-cell expansion and accumulation of CD8$^+$ and CD4$^+$ granzyme B$^+$ effector cells and FoxP3$^{pos}$/CD27$^{high}$/CD25$^{pos}$/CD127$^{low}$ CD4$^+$ T cells. CD8$^+$ cells down-regulated CD127 and BCl-2 and up-regulated Ki-67, consistent with a highly activated, proliferative profile. A cytokine storm also occurred, with GVHD-specific secretion of interleukin-1 receptor antagonist (IL-1Ra), IL-18, and CCL4. Costimulation Blockade and Sirolimus (CoBS) resulted in striking protection against GVHD. At the 30-day primary endpoint, CoBS-treated recipients showed 100% survival compared with no survival in untreated recipients. CoBS treatment resulted in survival, increasing from 11.6 to 62 days ($P < .01$) with blunting of T-cell expansion and activation. Some CoBS-treated animals did eventually develop GVHD, with both clinical and histopathologic evidence of smoldering disease. The reservoir of CoBS-resistant breakthrough immune activation included secretion of interferon-γ, IL-2, monocyte chemotactic protein-1, and IL-12/IL-23 and proliferation of cytotoxic T-lymphocyte–associated antigen 4 immunoglobulin-resistant CD28$^-$ CD8$^+$ T cells, suggesting adjuvant treatments targeting this subpopulation will be needed for full disease control. (*Blood*. 2010;116(24):5403-5418)**

## Introduction

Although haploidentical hematopoietic stem cell transplantation (HSCT) offers several important advantages to the sickest patients awaiting transplantation, it can result in substantial complications, including immune-incompetence after donor engraftment, graft rejection, and most prominently, graft-versus-host disease (GVHD). Although GVHD prophylaxis still largely relies on nonspecific immunosuppression, in the fields of autoimmunity and solid organ transplantation the past decade has witnessed a shift toward biologic therapies such as T-cell costimulation blockade, which are designed to more specifically target self- or alloreactive-T cells while preserving protective immunity.[1] Two of the most potent pathways of T-cell costimulation are the CD28:CD80/CD86 pathways and the CD40:CD154 pathways.[2-6] CD28-directed therapies have moved the farthest clinically, with the CD28-blockade agent cytotoxic T-lymphocyte–associated antigen 4 immunoglobulin (CTLA4Ig) approved for rheumatoid arthritis,[7] and a second-generation compound, belatacept, that has just completed phase 3 clinical trials for renal transplantation.[8] Although blockade of both sides of the CD40:CD154 pathway have shown promise in murine models of transplantation,[9-14] platelet-mediated thromboembolic complications have slowed clinical development of CD154-directed therapies.[15] Fortunately, several studies have shown that blockade of CD40 may also have significant potency for inhibiting alloreactivity while avoiding risks of thrombosis.[3,5,16,17] Importantly, although calcineurin inhibition may be antagonistic to costimulation blockade–based immunosuppression,[18-20] mammalian target of rapamycin inhibition with sirolimus is thought to be permissive for the abortive T-cell activation promoted by costimulation blockade.[18] Even though success with these approaches has been attained in many model systems, resistance to costimulation blockade also occurs. Thus, in murine models of bone marrow transplantation (BMT), costimulation blockade–resistant rejection

Submitted June 6, 2010; accepted August 22, 2010. Prepublished online as *Blood* First Edition paper, September 10, 2010; DOI 10.1182/blood-2010-06-289272.

*W.P.M. and S. Srinivasan contributed equally to this study.

The online version of this article contains a data supplement.

The publication costs of this article were defrayed in part by page charge payment. Therefore, and solely to indicate this fact, this article is hereby marked "advertisement" in accordance with 18 USC section 1734.

of donor BM was induced in the setting of virus-mediated memory T-cell expansion and heterologous immunity.[21] In addition, in both primate and clinical studies of solid-organ transplantation, significant rejection risks have been noted despite costimulation blockade, with adjunctive memory T cell–directed therapies sometimes required for prolonged allograft survival.[8,22,23] Furthermore, although anergy to GVHD-inducing alloantigens can be induced by ex vivo exposure of BM to recipient antigen-presenting cells (APCs) in the presence of CTLA4Ig,[24] in both murine and canine models of GVHD, results of investigations into the efficacy of in vivo CD28- and CD40-directed costimulation blockade have been mixed: both successes and failures have been documented for the inhibition of GVHD.[25-30] Understanding the mechanisms underlying both the successes and failures of costimulation blockade for GVHD prevention will be critical if this strategy is to be used widely in clinical transplantation.

To best facilitate the development of novel treatment paradigms for GVHD, a rigorous preclinical model is required. This model should be able to accomplish 2 critical tasks: it should permit a thorough dissection of the underlying immune mechanisms that control this disease, and it should facilitate the evaluation of emerging, clinically relevant, treatment strategies. Here, we report a novel primate model of GVHD that has allowed us, for the first time, to dissect the mechanisms controlling GVHD in this highly clinically relevant translational system. We find that primate GVHD is characterized both by rampant T-cell activation and by a compensating regulatory response and that combined costimulation blockade and sirolimus can significantly protect against GVHD even after high-risk haploidentical HSCT. However, our analysis indicates that the protection against GVHD afforded by costimulation blockade is not complete; by quantifying Ki-67 expression levels, we have identified a reservoir of breakthrough T-cell proliferation in the $CD28^-$ $CD8^+$ subpopulation. The degree to which these cells escaped from control with costimulation blockade/sirolimus correlated closely with the extent of clinical and histopathologic GVHD. These results identify Ki-67 expression as a powerful indicator of T-cell escape from immunosuppressive control and expose the $CD8^+/CD28^-$ subcompartment as a population that may require aggressive targeted immunosuppression for full inhibition of GVHD through costimulation blockade.

## Methods

### Experimental animals

This study used specific pathogen-free, juvenile rhesus macaques that were housed at the Yerkes National Primate Research Center. All animals were treated in accordance with Emory University and Yerkes National Primate Research Center Institutional Animal Care and Use Committee regulations.

### Creation of a major histocompatibility complex–defined rhesus macaque colony: microsatellite-based pedigree determination and major histocompatibility complex typing

We have completed an immunogenetic analysis on all potential transplant pairs, to perform major histocompatibility complex (MHC) haploidentical transplantation. The pedigree and MHC haplotype analysis, which have resulted in the creation of an MHC-defined rhesus macaque colony, are described in detail in supplemental Methods (available on the *Blood* Web site; see the Supplemental Materials link at the top of the online article).

### Creation of a rhesus macaque model of GVHD

Complete details of the HSCT protocol, pretransplantation preparation, posttransplanation immunosuppression, and supportive care, as well as the primate GVHD staging criteria, are described in supplemental Methods.

### Chimerism determination

When appropriate for specific donor-to-recipient mismatches, MHC- or sex-determining region Y–based chimerism was monitored by real-time SybrGreen PCR (polymerase chain reaction; ABI) as previously described.[22] If PCR-based chimerism determination was not possible, divergent donor- and recipient-specific microsatellite markers were used,[31] by comparing peak heights of the donor- and recipient-specific amplicons. T-cell chimerism was determined by sorting $CD3^+/CD20^-$ (T cells) with a FACSAria cell sorter (Becton Dickinson) before molecular analysis for donor-specific microsatellite amplicons or PCR products.

### GVHD histopathologic grading

At the time of necropsy, organs and tissues were paraffin-embedded, and then sections were cut and stained with hematoxylin/eosin or with an anti-CD3 antibody (Clone F7.2.38; Dako). Histopathologic scoring of GVHD used a semiquantitative scoring system (0.5-4.0 grades)[32] and was performed by an expert in GVHD histopathology (A.P.-M.), who was blinded to the treatment groups when analyzing the untreated and **Co**stimulation **B**lockade and **S**irolimus (CoBS)–treated recipients.

### Flow cytometric analysis

Multicolor flow cytometric analysis was performed on all transplant recipients, as described in detail in supplemental Methods.

### Multiplexed cytokine analysis

Multiplexed cytokine quantification from serum was performed with a Bio-Plex 200 (Bio-Rad) with the Milliplex non–human primate cytokine kit (Millipore).

## Results

### Efficient engraftment after MHC haploidentical HSCT in rhesus macaques

Eight of 9 recipients showed rapid and sustained donor engraftment after 8-Gy total body irradiation and HSCT (Table 1; Figure 1B-C). The single animal (R.8) that rejected the transplant received the lowest total nucleated cells of all the animals that received a transplant ($5.2 \times 10^8$/kg, compared with an average of $\sim 9 \times 10^8$/kg in the engrafted animals). In each of the other 8 animals that received a transplant, engraftment was rapid and resulted in full-donor chimerism in animals that did not receive posttransplant immunosuppression (Figure 1B R.1-R.3) and high-level chimerism in animals treated with immunosuppression ($> 80\%$ chimerism; Figure 1C). T-cell chimerism ranged from 96% to 100% in the untreated cohort and from 67% to 100% in animals treated long term with CoBS (Figure 1D animals R.4-R.7). At the time of his planned histopathologic analysis (day 20 after transplantation), R.9 had achieved 91% whole-blood chimerism and 45% T-cell chimerism.

### In the absence of immunosuppression, rhesus macaques developed rapid onset, clinically severe GVHD

The 3 animals who received haploidentical donor HSCs without posttransplantation immunosuppression (R.1-R.3) all developed rapid-onset clinical decline and clinical symptoms of severe

**Table 1. Summary of transplant and clinical characteristics**

| Animal | MHC disparity | Posttransplantation immunosuppression | Graft source | TNC/kg | $CD3^+$/kg | $CD34^+$/kg | Day of engraftment, donor cells > 25% | Day of death | Reason for euthanasia |
|---|---|---|---|---|---|---|---|---|---|
| R.1 | MHC haploidentical | None | PBSC | $5.5 \times 10^8$ | $1.7 \times 10^8$ | $1.7 \times 10^7$ | 7 | 7 | Severe clinical disability |
| R.2 | MHC haploidentical | None | PBSC | $7.7 \times 10^8$ | $2.2 \times 10^8$ | $1.8 \times 10^7$ | 6 | 6 | Severe clinical disability |
| R.3 | MHC haploidentical | None | BMT | $8.6 \times 10^8$ | $4.1 \times 10^7$ | $5.9 \times 10^7$ | 6 | 22 | Progressive clinical disability and weight loss |
| R.4 | MHC haploidentical | CTLA4Ig, anti-CD40 Ab, sirolimus | PBSC | $1.4 \times 10^9$ | $2.4 \times 10^8$ | $2.1 \times 10^7$ | 8 | 77 | Chronic decrease in activity, and acute clinical decline: CMV and GVHD detected on postmortem analysis |
| R.5 | MHC haploidentical | CTLA4Ig, anti-CD40 Ab, sirolimus | BMT + PBSC | $9.9 \times 10^8$ | $6.11 \times 10^7$ | $4.5 \times 10^7$ | 5 | 66 | Anorexia and weight loss |
| R.6 | MHC haploidentical | CTLA4Ig, anti-CD40 Ab, sirolimus | BMT | $1.1 \times 10^9$ | $5.5 \times 10^7$ | $3.3 \times 10^7$ | 5 | 63 | Anorexia and weight loss |
| R.7 | MHC haploidentical | CTLA4Ig, anti-CD40 Ab, sirolimus | BMT | $8.6 \times 10^8$ | $4.1 \times 10^7$ | $5.9 \times 10^7$ | 12 | 42 | Clinical decline, anorexia, and weight loss; GVHD detected on postmortem analysis |
| R.8 | MHC haploidentical | CTLA4Ig, anti-CD40 Ab, sirolimus | BMT | $5.2 \times 10^8$ | $1.3 \times 10^8$ | $3.0 \times 10^7$ | Rejected transplant | 64 | Anorexia and weight loss |
| R.9 | MHC haploidentical | CTLA4Ig, anti-CD40 Ab, sirolimus | BMT | $1.3 \times 10^9$ | $2.0 \times 10^7$ | $6.1 \times 10^7$ | 8 | 20 | Planned for timed histopathologic analysis |
| R.10 | Autologous transplant | CTLA4Ig, anti-CD40 Ab, sirolimus | PBSC | $2.3 \times 10^8$ | $3.2 \times 10^7$ | $1.5 \times 10^7$ | n/a | 35 | Planned for histopathologic analysis |
| R.11 | MHC matched | None | PBSC | $1.1 \times 10^9$ | $1.0 \times 10^8$ | $5.7 \times 10^7$ | 7 | 26 | Severe jaundice |

MHC indicates major histocompatibility complex; TNC, total nucleated cell; PBSC, peripheral blood stem cell; BMT, bone marrow transplantation; Ab, antibody; CMV, cytomegalovirus; and GVHD, graft-versus-host disease.

GVHD (Tables 1-3). The 2 animals receiving leukapheresis-derived transplants (recipients R.1 and R.2) succumbed to clinical complications more rapidly than the animal that received a BM-derived product (R.3). R.1 and R.2 became extremely ill by day 6 after transplantation, with a syndrome that included change in mental status, diarrhea, lassitude, and, in one of the animals, acute renal failure (R.1: serum creatinine = 8.2 μmol/L on the day of death). R.3 had slower onset of disease, but, similar to R.1 and R.2, this animal also developed diarrhea, anorexia, weight loss, and progressive lassitude. R.3 was also noted to have an erythematous rash, most prominent on the face, that began on day 12 after transplantation. The serum bilirubin rose in R.1, R.2, and R.3 (9-fold, 4-fold, and 7-fold over baseline, respectively), and all 3 animals had evidence of liver GVHD on histopathologic analysis (Table 3; Figure 2A). A single recipient (R.11) that received a transplant with MHC-matched stem cells without immunosuppression (and who lived until day 26 after transplantation; Table 1) showed a striking, acute increase in serum bilirubin between days 23 and 26 after transplantation, with a serum bilirubin of 393.4 μmol/L (23 mg/dL) (corresponding to stage IV clinical liver GVHD) in the setting of 100% whole-blood and 100% T-cell chimerism.

### Histopathologic analysis confirmed GVHD in all untreated animals

Similar to what was observed in the 1969 study of "secondary disease" in a cohort of non–MHC-defined macaques,[33] histopathologic analysis confirmed GVHD in each of the untreated recipients, with significant lymphocyte infiltration and loss of normal tissue architecture throughout the lungs, the liver, and the gastrointestinal (GI) tract (Figure 2A-B). Table 4 shows details of the individual tissue GVHD scores for the animals receiving haploidentical HSCT in comparison to an irradiation control, an autologous transplant control, and 2 normal, nonirradiated, animals not receiving a transplant. Although all untreated macaques had GI and liver abnormalities that were similar to that observed in human GVHD (diarrhea, jaundice, and increasing bilirubin), skin findings were inconsistent in rhesus macaque GVHD (not shown). Given the lack of correlation of skin findings with histopathologic GVHD, this organ was eliminated from histopathologic scoring of GVHD, with the total score consisting of analyses from the lungs, liver, and colon. Of note, a colon histopathologic score of 0.5 was seen in the irradiation and autologous transplantation controls, scores of 1-1.5 were seen in control animals not receiving a transplant, and scores of 2-3 were seen in the nontreated recipients of haploidentical transplants. Together, these data suggest that scores of $\geq 2$ were indicative of significant GI GVHD. In addition to GVHD in the liver, lungs, and colon, widespread tissue damage and T-cell infiltration was noted in untreated animals, including into the kidneys and the brain (not shown; S.S. and L.S.K., manuscript in preparation), consistent with uncontrolled T-cell proliferation and widespread tissue infiltration in the absence of immunosuppression.

### CD8-predominant lymphocyte expansion and activation correlated with the onset of clinical disease

To define the immunologic mechanisms controlling primate clinical GVHD, we monitored both cellular and serum immune phenotypes. As shown in Figure 3A-B we observed that within 1 week of transplantation, untreated peripheral blood stem cell (PBSC) recipients showed a rapid rise in the peripheral blood white blood cell (WBC) count, with predominant expansion of lymphocytes, and a concomitant rise in the absolute lymphocyte count

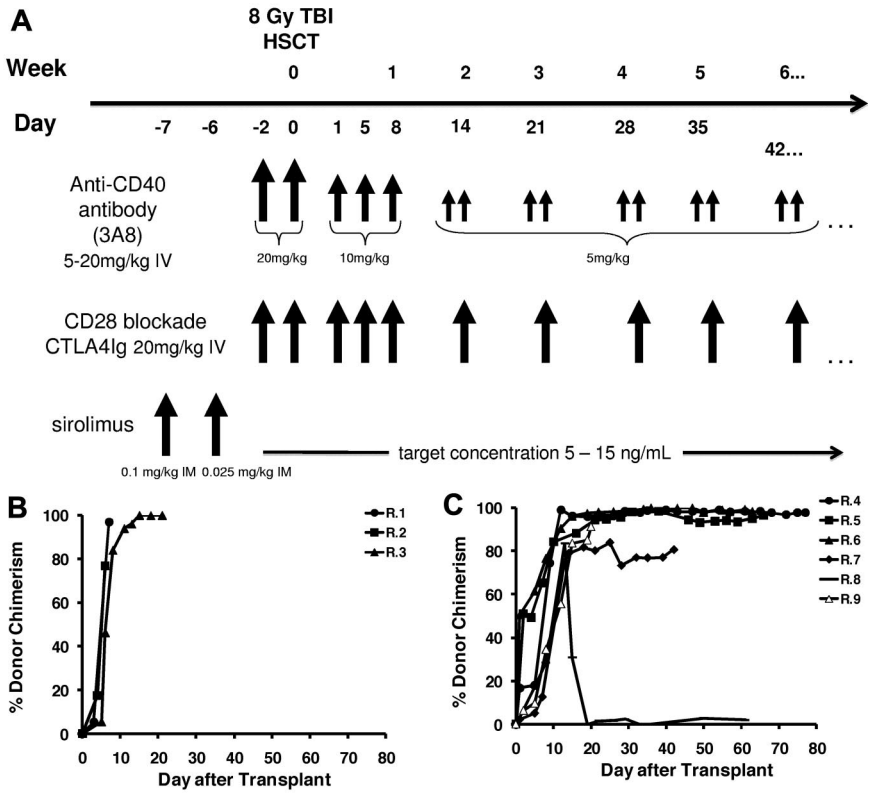


**Figure 1. High-level chimerism after rhesus HSCT.** (A) Rhesus macaque HSCT strategy. Each component of CoBS immunosuppression (anti-CD40 monoclonal antibody, CTLA4Ig, sirolimus) is shown, along with the total body irradiation (TBI)–based conditioning regimen. Control animals received only TBI-based conditioning but no posttransplantation immunosuppression. (B) Whole-blood chimerism in recipients who did not receive posttransplantation immunosuppression (R.1-R.3). (C) Whole-blood chimerism in recipients who received CoBS (R.4-9). (D) T-cell chimerism in the transplant recipients.

D

| Animal ID | T cell chimerism (day measured) |
|---|---|
| R.1 | 100% (7) |
| R.2 | 96% (6) |
| R.3 | 100% (22) |
| R.4 | 84% (57) |
| R.5 | 67% (43) |
| R.6 | 100% (34) |
| R.7 | 86% (40) |
| R.8 | 3% (29) |
| R.9 | 45% (20) |

(ALC; Figure 3A top 2 panels). R.3, who received a bone marrow transplant, had a slower rate of rise of the WBC count, with the absolute neutrophil count and ALC both beginning recovery after day 12 after transplantation (Figure 3A bottom). As shown in Figure 3B, the rise in the ALC occurred due to predominant $CD4^+$ and $CD8^+$ T-cell accumulation compared with little accumulation of $CD20^+/CD3^-$ B cells or $CD3^-/CD20^-/CD16^+/CD8^+$ natural killer cells. Although both $CD4^+$ and $CD8^+$ T cells exhibited significant accumulation, the $CD8^+$ T-cell expansion was the most striking, showing as much as a 2900-fold increase in the peripheral blood between days 3 and 7 (R.1; Figure 3B top). For each of the recipients in the untreated cohort (R.1-R.3), the engrafting T cells exhibited a blast-like phenotype, with significantly increased size and granularity (measured flow cytometrically by forward scatter/side scatter characteristics, and shown in a representative example in Figure 3C).

### Expanding donor $CD8^+$ and $CD4^+$ T cells shift toward distinct antigen-experienced phenotypes during primate GVHD

As has been previously reported for highly proliferating antiviral[34,35] and alloreactive[36] T cells, $CD8^+$ T cells showed decreased cell-surface expression of the interleukin-7 (IL-7) receptor, CD127, during GVHD induction (Figure 3D). In addition, the balance of $CD8^+$ T cells shifted from containing a significant proportion of

**Table 2. Clinical GVHD staging strategy**

| Stage | Skin | Liver (bilirubin) | Gastrointestinal tract | Activity (inversely related to GVHD) |
|---|---|---|---|---|
| 0 | No GVHD rash | < 4-fold increase over baseline | No diarrhea | Animal unable to respond normally to stimulation |
| 1 | Rash < 25% body surface area | 4- to 8-fold increase over baseline | "Mild" diarrhea with no other cause | Severely decreased or altered activity |
| 2 | Rash 25%-50% body surface area | 8- to 20-fold increase over baseline | "Moderate" diarrhea with no other cause | Moderately decreased or altered activity |
| 3 | Rash > 50% body surface area | 20- to 50-fold increase over baseline | "Severe" diarrhea with no other cause | Normal activity |
| 4 | Generalized erythroderma with bullous formation | > 50-fold increase over baseline | "Very severe" diarrhea with no other cause | |

GVHD indicates graft-versus-host disease.

**Table 3. Clinical GVHD staging in untreated animals**

| Animal | Skin | Liver | Gastrointestinal tract | Activity score |
|---|---|---|---|---|
| R.1 | 0 | 2 | 3 | 0 |
| R.2 | 0 | 1 | 2 | 0 |
| R.3 | 3 | 1 | 2 | 1.5 |

GVHD indicates graft-versus-host disease.

$CD28^+/CD95^-$ naive cells[37] toward a predominantly antigen-experienced, $CD95^+$ phenotype (average = 35% before transplantation, 94% at necropsy; Figure 3E-F). Within the $CD95^+/CD8^+$ subpopulation there was a skewing toward the $CD28^-$ subcompartment (increasing from an average of 24% of the $CD8^+$ T cells before transplantation to 67% at necropsy; Figure 3E-F). $CD4^+$ T cells exhibited a strikingly distinct shift in phenotype compared with $CD8^+$ T cells, preferentially expanding the $CD28^+/CD95^+$ subcompartment, with these cells increasing from an average of 41% before transplantation to 88% at necropsy (Figure 3E-F). In vitro analysis confirmed that both the $CD28^+$ and $CD28^-$ subpopulations could exhibit alloreactivity. Thus, as shown in Figure 3G, mixed lymphocyte reaction (MLR) analysis of unfractionated T cells showed substantial proliferation of both $CD28^+$ and $CD28^-$ subpopulations after a 5-day MLR culture. Furthermore, when the $CD28^+/CD95^-$, $CD28^+/CD95^+$, and $CD28^-/CD95^+$ populations were purified flow cytometrically before MLR analysis, each of the sorted populations could proliferate against alloantigens (Figure 3H).

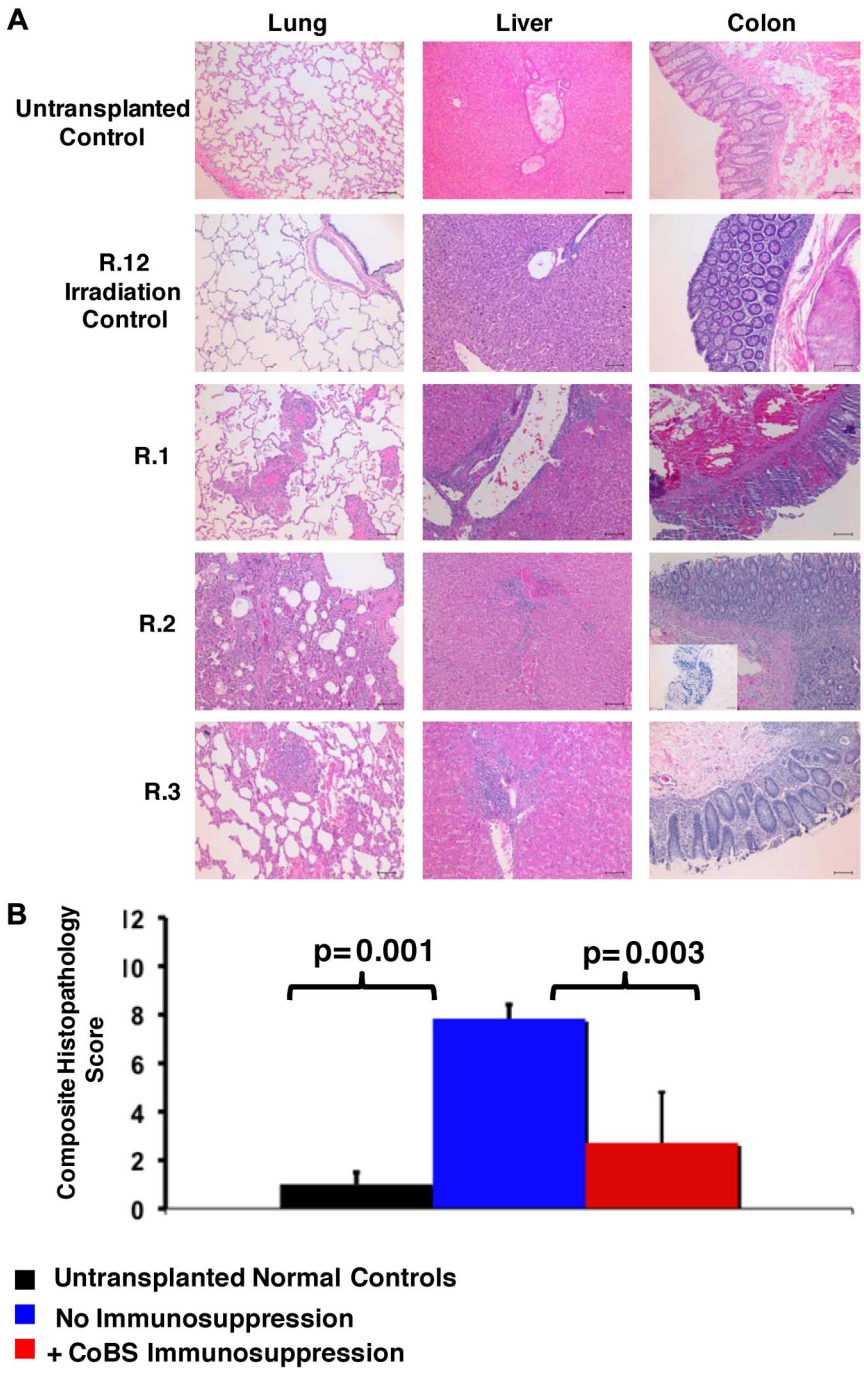


**Figure 2. Histopathologic evidence of GVHD in animals that received a transplant and no immunosuppression (R.1-R.3).** (A) Photomicrographs of hematoxylin and eosin (H&E) staining of the lungs, liver, and colon show GVHD in untreated animals. These studies used an Olympus BX51 microscope (Olympus America), using a 10×/0.40 UPlan Apo lens (Olympus). Slides were mounted with Permount solution (Sigma-Aldrich) and photographs were taken with the Spot RT Slider imaging system (Spot Imaging Solutions). Image analysis was performed using Spot Advanced Version 4.6 (Spot Imaging Solutions), and image processing was performed using Photoshop CS4 extended v11.01 (Adobe). (Row 1) A normal control that did not receive a transplant; (row 2) R.12, an irradiation control; (row 3) R.1; (row 4) R.2 (inset in the colon photomicrograph shows an example of CD3 staining of this organ); (row 5) R.3. Bar = 100 μm. (B) Untreated transplant recipients demonstrated significantly higher GVHD histopathology scores compared with either normal controls or CoBS-treated transplant recipients. Combined histopathologic GVHD scores for controls that did not receive a transplant (black), recipients of transplants without immunosuppression (blue), and recipients receiving CoBS immunosuppression (red) are shown. The histopathologic GVHD grading was performed by a pathologist blinded to the treatment regimens that the animals received. Individual tissue scores were from 0 (no GVHD) to 4 (severe GVHD), and the combined score was the sum of individual scores from the lung, liver, and colon.

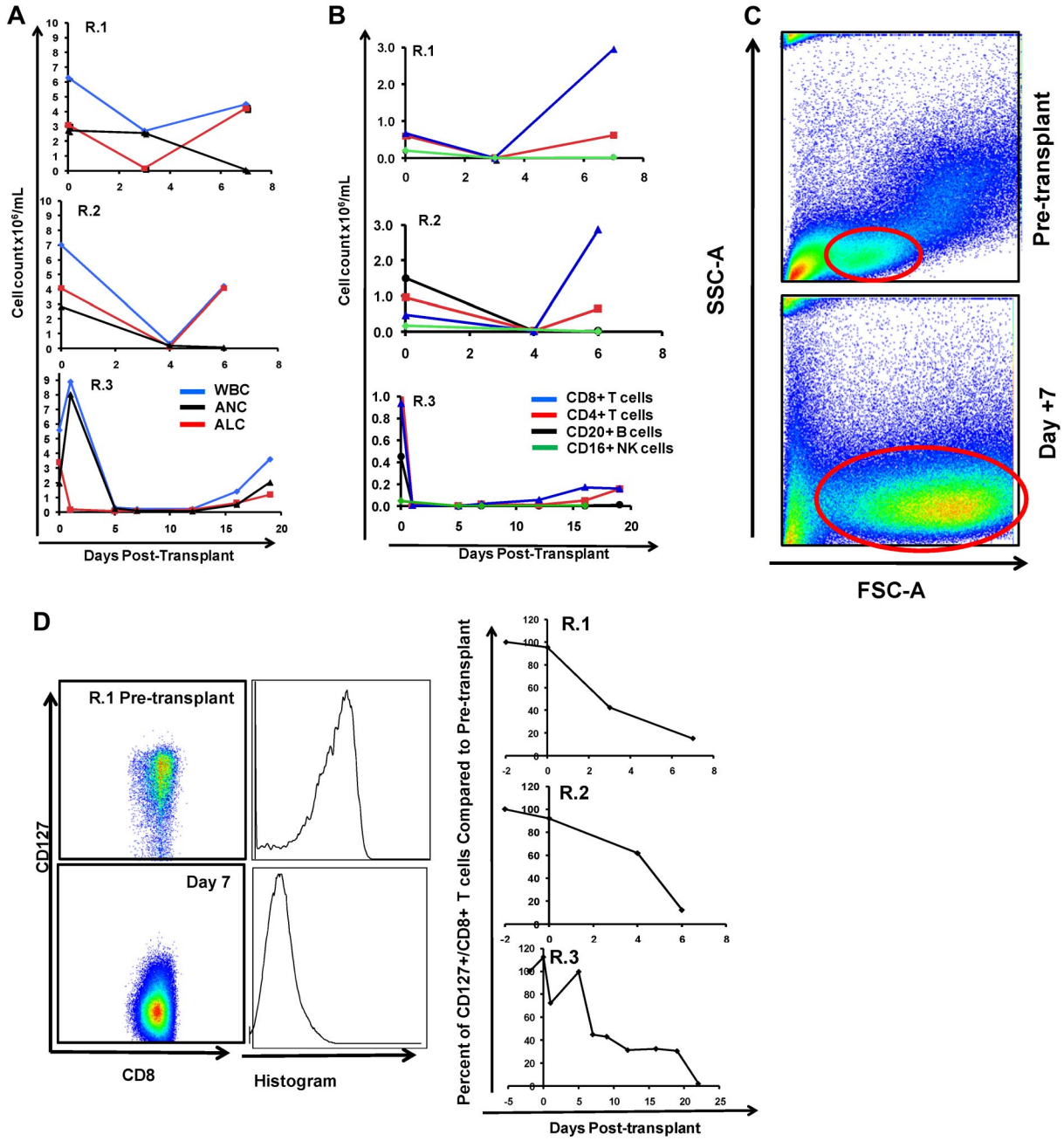


**Figure 3. The flow cytometric signature of primate GVHD.** (A) Longitudinal analysis of the white blood cell (WBC) count, absolute neutrophil count (ANC), and absolute lymphocyte count (ALC) in R.1-R.3. (B) Longitudinal analysis of the absolute CD8$^+$ T-cell count, the absolute CD4$^+$ T-cell count, the absolute CD20$^+$ B-cell count, and the absolute CD16$^+$ natural killer (NK) cell count in R.1-R.3. (C) Forward-scatter (FSC-A) versus side-scatter (SSC-A) flow cytometric analysis of the lymphocyte blast phenotype (red circle) in GVHD. Example from R.1 before transplantation (top) and on day 7 (bottom), during rapid T-cell expansion. (D) Down-regulation of CD127 in expanding CD8$^+$ T cells during GVHD. Panels on the left show pseudocolor dot plots and histogram analysis of CD127 expression on CD8$^+$ T cells analyzed both before transplantation (top) and on day 7 (bottom). Panels on the right show longitudinal analysis of CD127 expression on CD8$^+$ T cells in R.1-R.3, compared with pretransplantation expression levels of CD127.

Although in healthy rhesus macaques, the designation of T cells as either "central memory" or "effector memory" has been based on the level of CD28 expression in the CD95$^+$ antigen-experienced T-cell subcompartment,[37] in the context of the explosive alloactivation and T-cell expansion that occurred with no prophylaxis during GVHD, the CD95$^+$ subcompartment probably contained more effector cells than memory cells. Thus, in R.1-R.3, the expanding CD95$^+$ population had been very recently exposed to stimulating alloantigens, was proliferating rapidly (Figure 3B-C), and showed a massive up-regulation of the effector molecule granzyme B in both the CD28$^+$ and CD28$^-$ subpopulations (Figure 3I). Although some of these cells were probably programmed to eventually become bone fide memory cells, in the short time period before GVHD-induced mortality, the effector phase of T-cell pathology[38] probably predominated.

### Changes in Ki-67 and BCl-2 accompany GVHD

Consistent with their activated, proliferative effector phenotypes, both CD4$^+$ and CD8$^+$ T cells exhibited striking shifts in expression

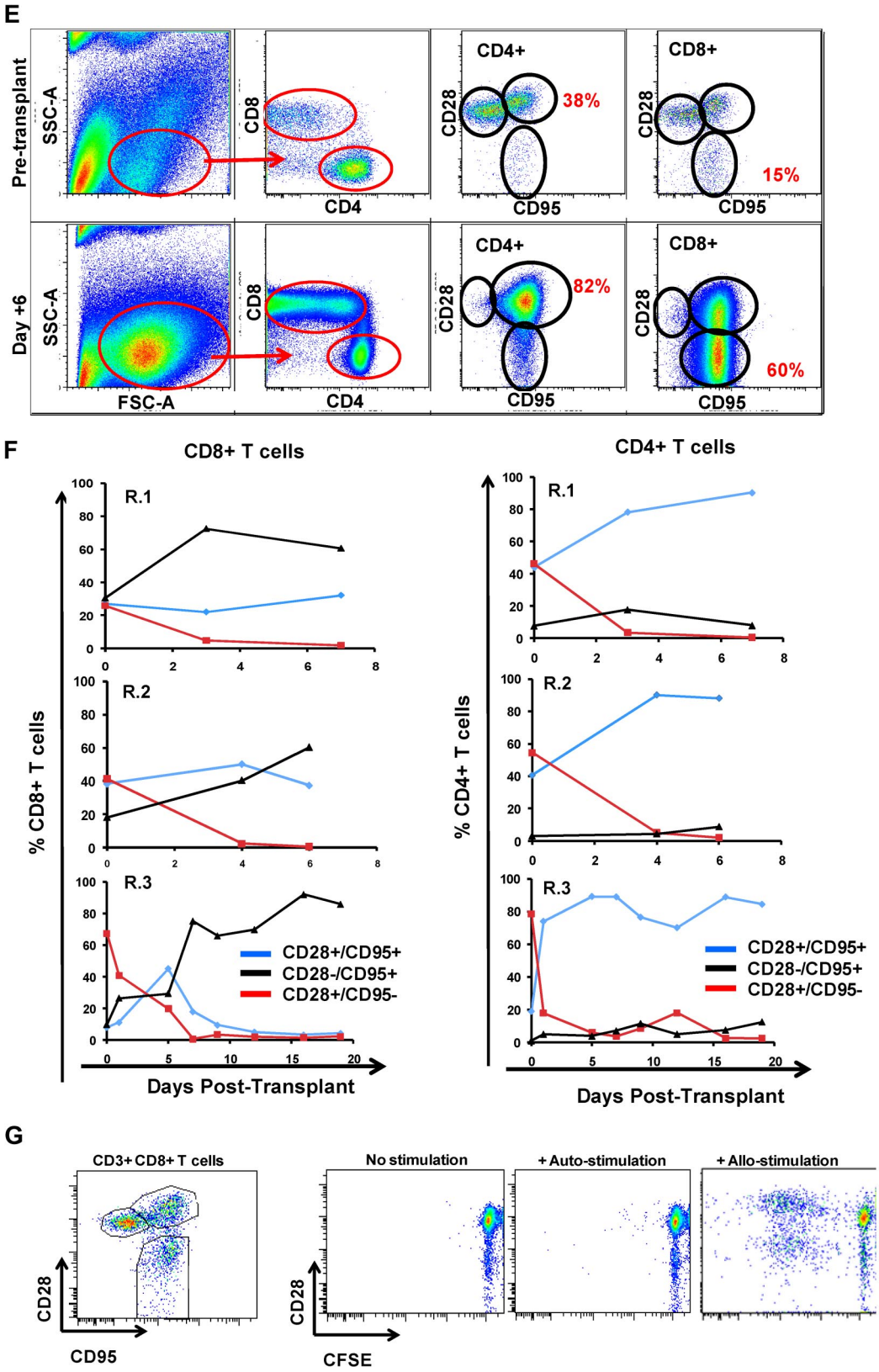


**Figure 3 (continued).** (E) Representative flow cytometric analysis of R.2, showing the phenotypic shift away from naive T cells that occurred in both $CD4^+$ and $CD8^+$ compartments during GVHD; before transplantation (top), day 6 after transplantation (bottom). (Third column from the left, top, and bottom) Example of $CD4^+$ T cells shifting to a $CD28^+/CD95^+$ predominant phenotype after transplantation (compare top with bottom rows). (Fourth column from the left) Example of $CD8^+$ T cells shifting to a $CD28^-/CD95^+$ predominant phenotype after transplantation (compare top with bottom rows). (F) Longitudinal analysis of $CD4^+$ and $CD8^+$ T-cell subsets during GVHD. R.1-R.3 all shift toward a predominant $CD28^-/CD95^+$ $CD8^+$ phenotype (left) and a predominant $CD28^+/CD95^+$ $CD4^+$ phenotype (right). (G) Representative CFSE (5,6-carboxyfluorescein diacetate, succinimidyl ester) MLR analysis of the proliferation of $CD28^+$ and $CD28^-$ $CD8^+$ T cells. (Left) Representative flow cytometric analysis of $CD3^+/CD8^+$ T cells showing the CD28 and CD95 phenotypes. (Right) CFSE MLR analysis after a 5-day MLR culture. Minimal proliferation occurred in cultures incubated without any stimulators ("No stimulation") or those incubated with autologous stimulator cells ("+ Auto-stimulation"). However, in those incubated with allogeneic PBMCs ("+ Allo-stimulation), proliferation occurred in both $CD28^+$ and $CD28^-$ subpopulations. The results shown are representative of $\geq 5$ separate MLR assays with the use of distinct donor:recipient pairs.

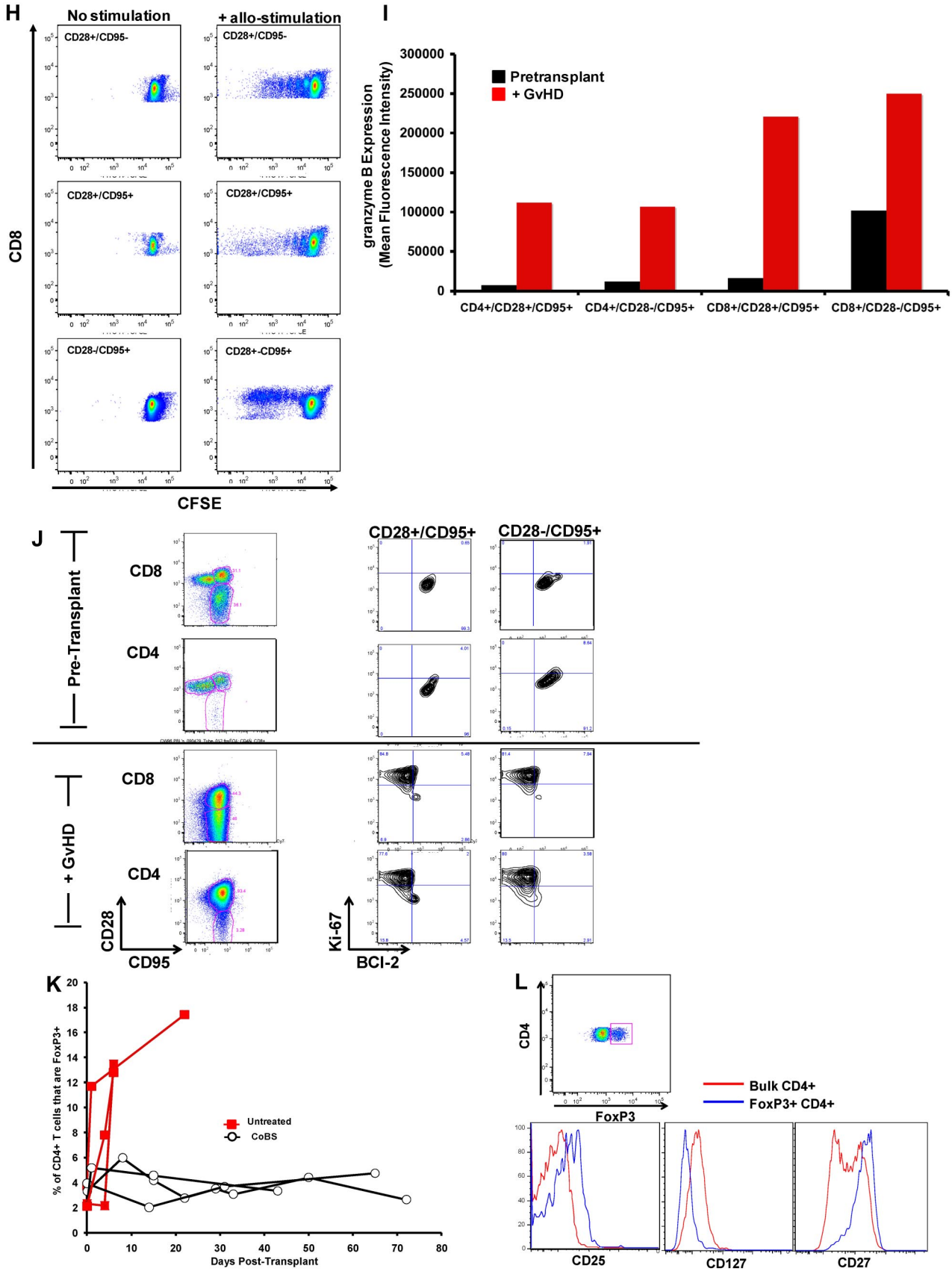


**Figure 3 (continued).** (H) CFSE MLR analysis of flow cytometrically sorted CD28$^+$ and CD28$^-$ populations. CD28$^+$/CD95$^-$, CD28$^+$/CD95$^+$, and CD28$^-$/CD95$^+$ CD8$^+$ T cells were sorted with a FACSAria flow cytometer before CFSE MLR analysis either in the absence (left) or presence (right) of allogeneic stimulator cells. Shown are representative CFSE proliferation profiles from 1 of 3 replicate experiments. (I) Granzyme B expression is highly up-regulated during GVHD. Shown is a representative example of the mean fluorescence intensity of granzyme B in both CD28$^+$/CD95$^+$ and CD28$^-$/CD95$^+$ subpopulations for CD4$^+$ and CD8$^+$ T cells; granzyme B fluorescence before transplantation (black), granzyme B fluorescence at the time of necropsy in the setting of severe clinical GVHD (red). (J) BCl-2 and Ki-67 show significant shifts in expression during GVHD.

**Table 4. Histopathologic GVHD scores**

| Animal | Treatment regimen | Lung | Liver | Colon | Total score | Average total score ± SD |
|---|---|---|---|---|---|---|
| R.1 | No treatment | 2 | 2.5 | 3 | 7.5 | 7.83 ± 0.58 |
| R.2 | No treatment | 3 | 2.5 | 2 | 7.5 | |
| R.3 | No treatment | 4 | 2.5 | 2 | 8.5 | |
| R.4 | CoBS | 3 | 0.5 | 3 | 6.5 | 3 ± 2.12 |
| R.5 | CoBS | 0 | 0 | 1.5 | 1.5 | |
| R.6 | CoBS | 0 | 0.5 | 1 | 1.5 | |
| R.7 | CoBS | 1 | 1 | 1.5 | 3.5 | |
| R.9 | CoBS | 1 | 0.5 | 0.5 | 2 | |
| R.10 | Autologous transplantation | 0.5 | 0.5 | 0.5 | 1.5 | NA |
| R.11 | No treatment, MHC matched | 3.5 | 3 | 1.5 | 8 | NA |
| R.12 | Irradiation control | 0 | 0 | 0.5 | 0.5 | NA |
| | Normal animal, no irradiation | 0 | 0 | 1 | 1 | 1.25 ± 0.35 |
| | Normal animal, no irradiation | 0 | 0 | 1.5 | 1.5 | |

GVHD indicates graft-versus-host disease; CoBS, costimulation blockade and sirolimus; NA, not applicable; and MHC, major histocompatibility complex.

of BCl-2 and Ki-67[39-42] during GVHD. Thus, as shown in Figure 3J, BCl-2/Ki-67 flow cytometry showed a quiescent pattern before transplantation, with high expression of BCl-2 and low expression of Ki-67, in naive (not shown), $CD28^+/CD95^+$, and $CD28^-/CD95^+$ subpopulations for both $CD4^+$ and $CD8^+$ T cells. However, on the development of GVHD, both $CD4^+$ and $CD8^+$ T cells down-regulated the antiapoptotic protein BCl-2 (as much as 10-fold and 8-fold for $CD4^+$ and $CD8^+$ T cells, respectively) and up-regulated the proliferation marker Ki-67 (as much as 5-fold and 7-fold for $CD4^+$ and $CD8^+$ T cells, respectively), consistent with the development of globally activated and proliferating T cells.

### Expansion of FoxP3$^+$ CD4$^+$ T cells during GVHD

As shown in Figure 3K, in addition to the documented expansion of effector T-cell populations in animals that developed GVHD, these recipients also showed an increase in the percentage of $CD4^+$ T cells expressing the FoxP3 transcription factor. Although it has been reported that rapidly cycling $CD4^+$ T cells can express FoxP3 without acquiring true regulatory function,[43] our previous work has shown that, when expanded in vitro with the use of CD3/CD28 ligation, primate effector $CD4^+$ T cells did not express FoxP3.[44] Furthermore, the expanding $FoxP3^+$ population observed in untreated animals bore other flow cytometric hallmarks of regulatory cells: As shown in Figure 3L, they showed higher expression of CD25 and CD27 but decreased expression of CD127. Given that the animals who developed GVHD died rapidly, while they were still lymphopenic, it was not technically possible to acquire sufficient flow-sorted putative regulatory cells from these animals to verify their suppressor function with the use of in vitro suppression assays.[22] Thus, these results cannot be taken as proof that $CD4^+$ T cells with regulatory function expanded during GVHD. However, they are suggestive that counter-regulatory forces may be activated during the rapid, T-cell expansion and severe tissue destruction that occurs during untreated GVHD.

### Secretion of IL-18, IL-1 receptor antagonist, interferon γ, and CCL4 is associated with GVHD

Using multiplexed flow cytometric serum cytokine analysis, we interrogated the profile of cytokine secretion in the animals that received a transplant. These data are depicted in Figure 4A-C. Of the 23 cytokines analyzed (interferon γ [IFN-γ], tumor necrosis factor α, transforming growth factor α, IL-1β, IL-2, IL-4, IL-5, IL-6, IL-8, IL-10, IL-12/23 (p40), IL-13, IL-15, IL-17, IL-18, IL-1 receptor antagonist [IL-1RA], monocyte chemotactic protein 1, macrophage-inflammatory protein 1, CCL4, vascular endothelial growth factor, CD40L, granulocyte colony-stimulating factor, granulocyte-macrophage colony-stimulating factor), we found that 4 were highly secreted in animals who developed GVHD: IL-1RA, IL-18, IFNγ, and CCL4. Furthermore, these cytokines were secreted into the serum at a tempo that mirrored the tempo of GVHD (Figure 4A). Thus, R.1 and R.2, who each received a transplant with peripheral blood stem cells, secreted these cytokines early, whereas R.3, who received a BM transplant, secreted them more slowly, consistent with the slower onset of GVHD in this animal. Although the pattern of IL-8 secretion, a recognized human biomarker of GVHD,[45] was complex (Figure 4B), it was observed to be elevated early in all 3 of the untreated recipients and to accumulate to the highest extent in R.4 and R.7, the CoBS-treated animals who showed the highest histopathologic GVHD scores (Table 4). Finally, several cytokines were notable for their lack of significant accumulation in the serum, either during GVHD or with CoBS immunosuppression (Figure 4C). These include tumor necrosis factor, IL-1β, IL-17, IL-10, and transforming growth factor. The lack of IL-17 may not be unexpected, given that cytokine analysis was performed in the serum, and this cytokine is thought to act locally during infiltration of Th17 cells into target organs.[46,47] The primate model will allow us to specifically examine the role that Th17 cells play in target-organ infiltration, such that their tissue-specific role in GVHD can be rigorously determined.

**Figure 3 (continued).** (Top) Representative analysis from R.2, before transplantation. (Bottom) Day 6 after transplantation. (Left) T-cell subpopulations are first identified with CD28 and CD95 staining. The $CD28^+/CD95^+$ and $CD28^-/CD95^+$ cells were then queried for their expression of BCl-2 and Ki-67 (right). (K) $CD4^+/FoxP3^+$ cells expanded during GVHD in rhesus macaques. (Red) Longitudinal analysis of $CD4^+/FoxP3^+$ T-cell homeostasis in the untreated animals R.2, R.3, as well as a third MHC-disparate transplant recipient (R.1 could not be evaluated because of a technical problem with FoxP3 staining on the day of death). (Black) Longitudinal analysis of $CD4^+/FoxP3^+$ T-cell homeostasis in the CoBS-treated animals, R.4, R.5, and R.7 (R.6 could not be evaluated because of technical problems with CD3/CD4 staining for this animal). (L) $FoxP3^+/CD4^+$ T cells (gated population, and blue traces on the histograms) showed up-regulation of CD25, down-regulation of CD127, and up-regulation of CD27 compared with $FoxP3^-/CD4^+$ T cells (red traces).

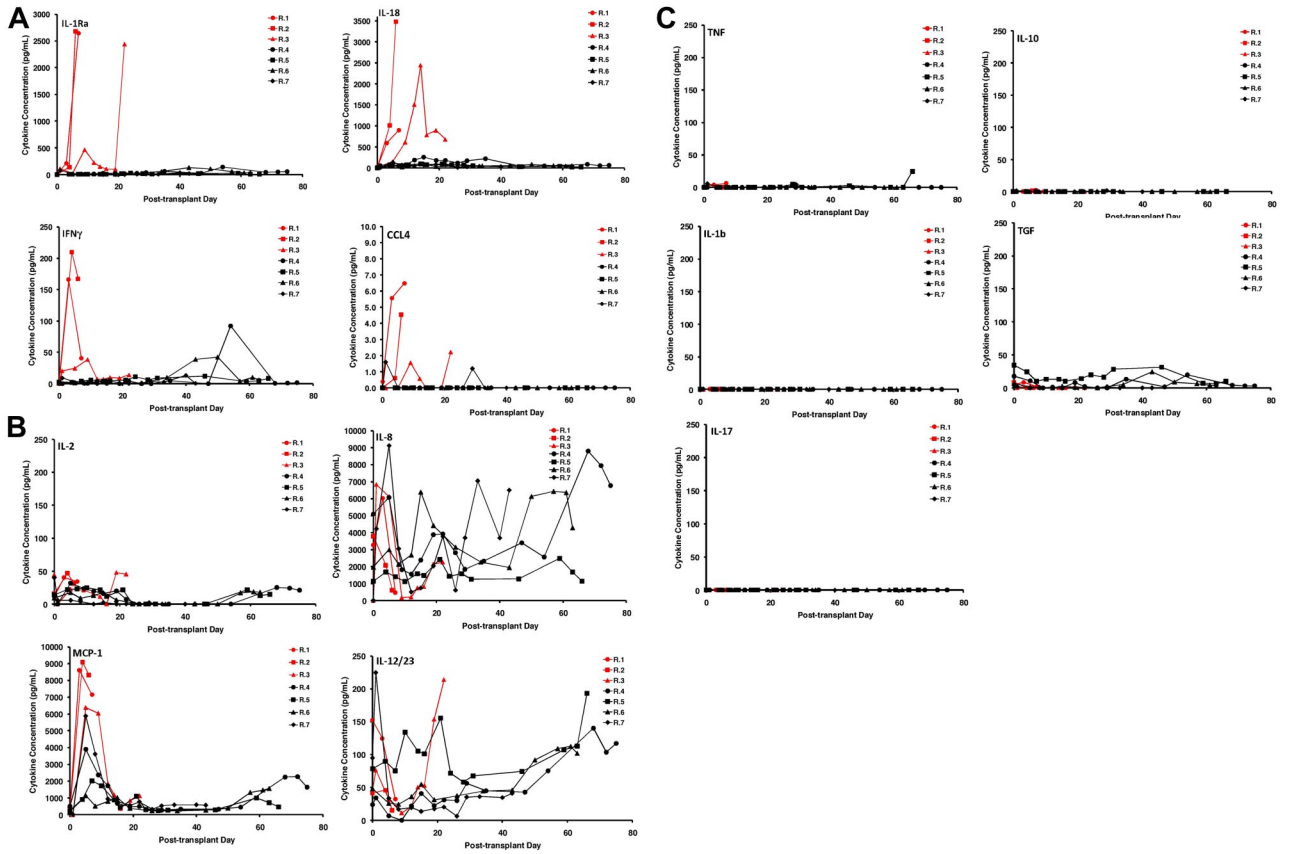


**Figure 4. Multiplexed luminex analysis shows a GVHD-specific cytokine secretion profile.** (A) Secretion patterns of IL-1RA, IL-18, IFNγ, and CCL4 in both untreated (red traces) and CoBS-treated (black traces) transplant recipients. (B) Secretion patterns of IL-2, IL-8, monocyte chemotactic protein 1 (MCP-1), and IL-12/23 in both untreated (red traces) and CoBS-treated (black traces) transplant recipients. (C) Secretion patterns of tumor necrosis factor, IL-10, IL-1β, transforming growth factor (TGF), and IL-17 in both untreated (red traces) and CoBS-treated (black traces) transplant recipients.

### Animals receiving CoBS were protected from the early T-cell expansion associated with GVHD and showed 100% survival at the 30-day primary clinical endpoint

Table 1 summarizes the transplantation characteristics of the 6 animals who received CoBS immunosuppression in the setting of MHC haploidentical HSCT. Despite rapid donor engraftment in 5 of 6 recipients and significant donor T-cell chimerism (Figure 1C-D), T-cell activation was significantly controlled in the CoBS-treated cohort (Figure 5). The blast phenotype observed in animals developing GVHD was absent, with lymphocytes retaining their pretransplantation forward-scatter and side-scatter flow cytometric characteristics (Figure 5A). Although CoBS-treated recipients recovered both the total WBC count and the absolute neutrophil count, these recipients showed a consistent delay of ALC recovery, with lymphocyte counts suppressed for the duration of treatment with CoBS (Figure 5B red traces). This inhibition of T-cell proliferation was associated with a striking survival advantage when CoBS-treated animals were compared with untreated animals at the 30-day primary endpoint, with 100% survival observed in the CoBS-treatment arm compared with 0% survival in the untreated recipients ($P = .01$; Figure 5C).

### CoBS significantly, albeit incompletely, protected recipients from clinical GVHD

According to the study design (described in supplemental Methods), after the 30-day primary endpoint was reached successfully, observation of the CoBS-treated cohort was extended such that overall survival could be determined. As shown in Table 5, even when the analysis was extended long term, there was limited diarrhea, no widespread skin rash, and no elevation of bilirubin in CoBS-treated recipients. However, despite the striking protection afforded by CoBS, all 4 of the CoBS-treated animals ultimately showed various degrees of posttransplantation disability, anorexia, and weight loss, with the mean survival time for the CoBS-treated cohort being 62 days, compared with 11.6 days for the untreated animals ($P = .01$; Figure 5D). Evidence from control transplantations suggests that in the setting of the limited nutritional supportive care that was provided to transplant recipients in this study, irradiation-induced GI toxicity probably contributed to the anorexia and weight loss observed in CoBS-treated recipients. Thus, R.8 (the animal who rejected the transplant), R.10 (the autologous transplant recipient), and R.12 (the irradiation control) all showed significant anorexia, whereas historical controls, who received a transplant with a nonmyeloablative busulfan-based preparative regimen, in the setting of CoBS immunosuppression, maintained normal appetites and weight (not shown). However, clinical,

**Table 5. Clinical GVHD staging in CoBS-treated animals**

| Animal | Skin | Liver | Gastrointestinal tract | Activity |
|---|---|---|---|---|
| R.4 | 0 | 0 | 2 | 1.6 |
| R.5 | 0 | 0 | 0.5 | 2.2 |
| R.6 | 1 | 0 | 1 | 2.5 |
| R.7 | 1 | 0 | 0 | 1.9 |

GVHD indicates graft-versus-host disease; and CoBS, costimulation blockade and sirolimus.

histopathologic, and flow cytometric data indicate that in addition to regimen-related toxicities, breakthrough GVHD also ultimately developed in some of the CoBS-treated animals. Thus, histopathologic analysis showed breakthrough lymphocytic infiltration into the colon, the lungs, and the liver, most prominently in R.4 and R.7 (Table 4; Figure 5E), consistent with smoldering GVHD. These animals also showed signs of posttransplantation clinical disability, which correlated closely with their degree of GVHD histopathology. Thus, as described in supplemental Methods, the well-being of the transplant recipients was measured daily with the use of an activity score (ranging from a score of 0 for extreme disability to a score of 3 for normal activity). Clinical disability was associated with a daily activity score of $< 2$. As shown in Figure 5F, the extent to which each of the transplant recipients (in both the untreated and the CoBS-treated cohorts) showed clinical disability correlated closely with the histopathologic GVHD score. For the untreated recipients (R.1-R.3; Table 1), the clinical decline was severe enough that it necessitated euthanasia. For the CoBS-treated recipients R.5, R.6, and R.7, animal-welfare end points were reached predominantly due to weight loss, which ultimately reached $> 25\%$ of their pretransplantation weight (Figure 5G). Although R.4 also showed anorexia and weight loss, this animal was euthanized on the basis of poor clinical condition, showing an acute rapid decline overlying his chronic disability, and was found postmortem to have cytomegalovirus reactivation, in addition to significant GVHD.

Multiplexed flow cytometric analysis showed significant but incomplete protection from T-cell activation in CoBS-treated recipients. Figure 6A shows that, despite the significant inhibition of T-cell proliferation that CoBS-treatment produced, these animals did experience shifts in T-cell phenotype, most prominently in the $CD4^+$ T-cell subcompartment, which shifted toward $CD28^+/CD95^+$ predominance after transplantation. The T-cell subpopulation balance was more variable for $CD8^+$ T cells. Thus, as shown for the representative recipients R.4 and R.5 (Figure 6A), in some animals there was a modest increase in the proportion of $CD8^+$ $CD28^-/CD95^+$ cells after transplantation (R.4, which increased from 20% $CD28^-/CD95^+$ cells before transplantation to 50% at necropsy), whereas other animals showed stable proportions of $CD28^-/CD95^+$ $CD8^+$ subpopulations (R.5; Figure 6A; 42% before transplantation, 39% at necropsy). Unlike in the untreated recipients, in whom naive T cells strikingly disappeared from the peripheral blood after transplantation (Figure 3F), CoBS-treated animals were better able to maintain a cohort of naive $CD4^+$ and $CD8^+$ T cells (Figure 6A red traces), despite widespread exposure of these T cells to recipient-derived alloantigen. In addition, the $CD8^+$ T cells in CoBS-treated recipients better maintained CD127 expression (Figure 6B), in contrast to the striking loss of CD127 observed in the highly activated $CD8^+$ T cells in the untreated cohort (Figure 3D). The preservation of CD127 was not complete, however, as shown in Figure 6B, whereas R.4, R.5, and R.6 all showed stable CD127 expression, and R.7, who exhibited the most rapid weight loss and anorexia of the treated cohort (and who experienced a period of subtherapeutic sirolimus levels from day 29 through 42; Figure 6C), exhibited significant loss of CD127 on $CD8^+$ T cells.

### BCl-2/Ki-67 flow cytometry showed breakthrough activation in the $CD8^+/CD28^-/CD95^+$ subpopulation

In contrast to the untreated animals, who showed global down-regulation of BCl-2 and up-regulation of Ki-67 in all $CD4^+$ and $CD8^+$ T subpopulations (Figure 3I), CoBS-treated animals showed significant protection from this GVHD-associated flow cytometric signature, with one important exception. As shown for R.4 in Figure 6D, although the $CD4^+$ T-cell subpopulations ($CD28^+/CD95^+$ and $CD28^-/CD95^+$) displayed quiescence as measured by BCl-2/Ki-67 expression, for $CD8^+$ T cells, a different pattern emerged. Although the $CD28^+$ $CD8^+$ T-cell subpopulations (both $CD95^-$ and $CD95^+$) both largely maintained the BCl-$2^{high}$/Ki-$67^{low}$ quiescent phenotype, a significant proportion of the $CD28^-/CD95^+$ cells down-regulated BCl-2 and up-regulated Ki-67, consistent with an activated, proliferative phenotype.[42,48,49] These results are consistent with an in vitro analysis that showed the diminished ability of CTLA4Ig to inhibit alloproliferation in $CD28^-/CD95^+$ T cells. Thus, as shown for the representative example in Figure 6E, all 3 T-cell subpopulations ($CD28^+/CD95^-$, $CD28^+/CD95^+$, and $CD28^-/CD95^+$) proliferated after coculture with allogeneic stimulators in the absence of CTLA4Ig treatment. However, although treatment with CTLA4Ig significantly inhibited proliferation in the $CD28^+/CD95^-$ and $CD28^+/CD95^+$ subpopulations (0.5% and 1.3% proliferation, respectively, with CTLA4Ig compared with 6.9% and 79.6% proliferation, respectively, without CTLA4Ig), the $CD28^-/CD95^+$ cells were still capable of significant alloproliferation (38% proliferation with CTLA4Ig, 31% proliferation without CTLA4Ig). Of note, a strong correlation was observed between the degree of Ki-67 up-regulation in $CD8^+/CD95^+/CD28^-$ T cells and the degree of GVHD-associated histopathology (Figure 6F), suggesting that this flow cytometric profile, accessible in the peripheral blood, may be predictive of GVHD severity.

Breakthrough immune activation was also evident when cytokine secretion was examined. Thus, although CoBS-treated animals showed significantly less secretion of 3 of the cytokines associated with untreated GVHD (IL-1RA, IL-18, and CCL4; Figure 4A), they did eventually secrete a collection of cytokines, concomitant with their clinical decline. Thus, as shown in Figure 4A-B, IFNγ, IL-2, IL-8, monocyte chemotactic protein 1, and IL-12/23 all eventually accumulated in the serum of CoBS-treated recipients, suggesting that the secretion of these cytokines may also signal escaped immune activation despite costimulation blockade/sirolimus.

## Discussion

In this report, we describe the creation of an MHC-defined primate model of HSCT. This model is expected to offer several unique advantages compared with existing murine models of GVHD. Thus, although the established murine models allow critical mechanistic questions to be addressed in a systematic, high throughput fashion, they also have significant limitations, especially with respect to the rapid translation of results to clinical situations: Thus, rodents are in-bred and housed in specific pathogen-free conditions and are well-documented to have a much more easily controlled alloresponse than either primates or patients. In addition, their response to tissue injury after conditioning, the kinetics of lympho-myelopoietic recovery, as well as the expression pattern of CD28, are significantly different from patients. These distinctions decrease the predictive power of studies performed only in rodent models and underscore the importance of the creation of an MHC-defined primate model of GVHD. Indeed, the studies described in this article were designed, in part, to provide preclinical data for the first clinical trial of CTLA4Ig for in vivo GVHD prevention, which has recently been opened for enrollment (http://clinicaltrials.gov/ct2/show/NCT01012492).

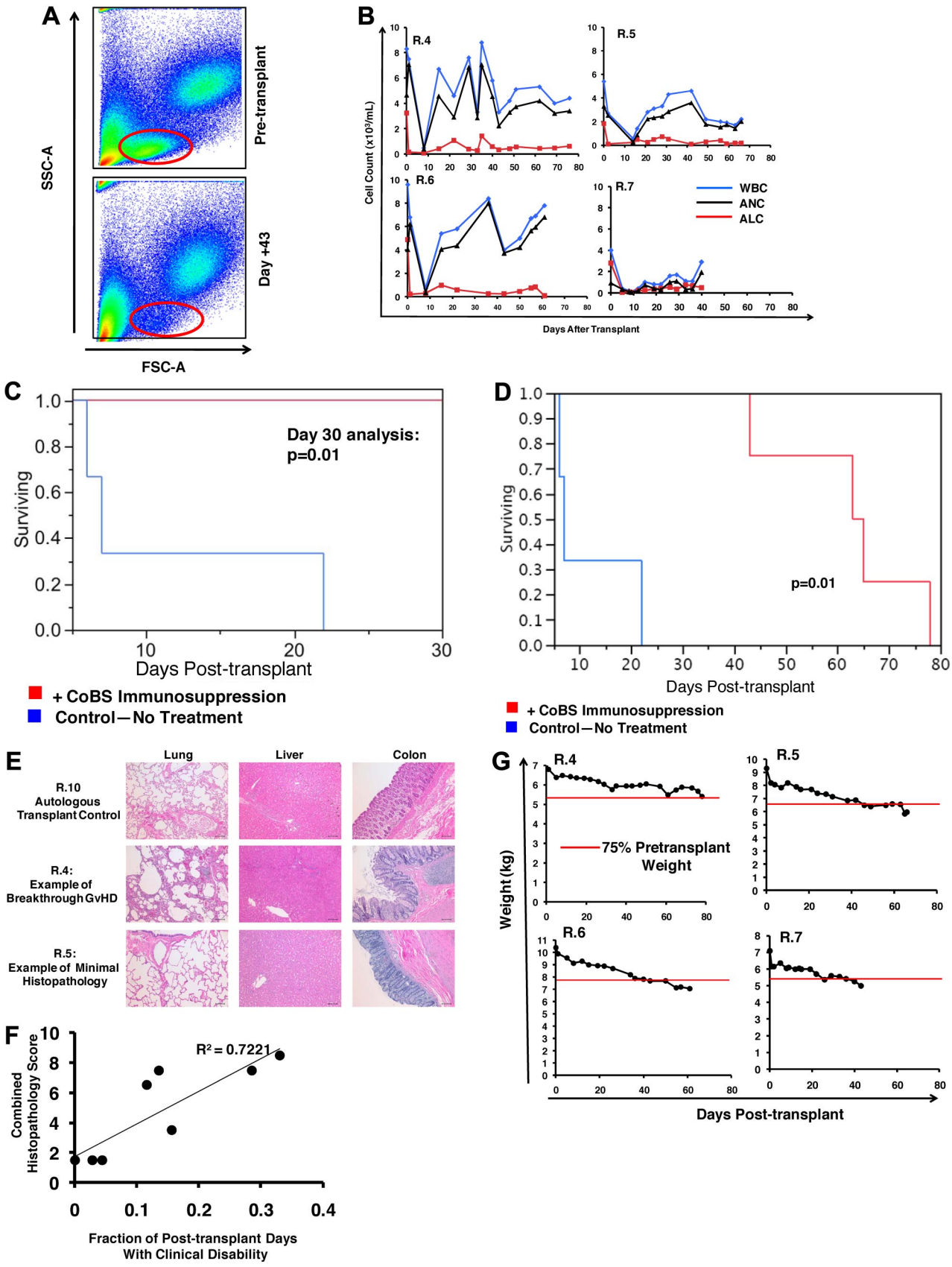


Figure 5.

We find that primate GVHD is associated with rampant T-cell proliferation and activation. We have identified CD4- and CD8-specific phenotypic conversions that occur after transplantation, as well as a pattern of cytokine secretion that accompanies GVHD.

We show that combined costimulation blockade and sirolimus offers significant protection against GVHD, with treated recipients showing 100% survival at 30 days after transplantation, despite high-risk haploidentical HSCT. Given the design of this study, which included neither intensive nutritional supportive care nor rescue treatment for GVHD symptoms, this survival advantage probably indicates significant anti-GVHD activity of combined costimulation blockade and sirolimus. Some of the treated animals did eventually develop both clinical and histopathologic signs of smoldering GVHD, which correlated with a flow cytometric signature consistent with breakthrough T-cell activation in the CTLA4Ig-resistant $CD28^-$ $CD8^+$ T-cell subcompartment.

Several novel insights into GVHD cellular and molecular pathogenesis have been gained from this study. Our results show the following. (1) Donor T-cell expansion is accompanied by distinctive $CD4^+$ and $CD8^+$ T-cell subpopulation shifts, with $CD4^+$ T cells taking on a predominantly $CD28^+$ phenotype, and $CD8^+$ T cells taking on a predominantly $CD28^-$ phenotype. (2) GVHD is accompanied by a striking down-regulation of CD127 on $CD8^+$ T cells, similar to what has been observed in viral models of T-cell activation. (3) GVHD is associated with reduced expression of BCl-2 and increased expression of both granzyme B and Ki-67 in all T-cell subpopulations, with the up-regulation of Ki-67 correlating with clinical GVHD severity. (4) In the absence of immunoprophylaxis, GVHD is also potentially associated with a compensatory regulatory response, with the elaboration of inhibitory cytokines (including significant accumulation of IL-1RA in the serum), and the expansion of $FoxP3^+/CD4^+$ T cells, which, although not proven in this study, may also have regulatory function. Previous clinical observations have suggested that this regulatory response may also exist in patients, in whom increased $CD4^+$ T-cell apoptosis was observed in those who developed grade II-IV GVHD.[50]

Having established a multimodal analysis strategy for primate GVHD pathogenesis, we were able to determine the effect of a novel immunosuppressive strategy from both a clinical and mechanistic standpoint. We found that even after haploidentical transplantation, animals treated with CoBS immunosuppression lived significantly longer and were free of the severe, systemic symptoms of GVHD that rapidly developed in the untreated cohort. Although CoBS was able to significantly inhibit the explosive T-cell activation that occurred in untreated animals, GVHD did, nonetheless, develop in some treated animals. Using flow cytometric analysis of BCl-2 and Ki-67, we identified a reservoir of breakthrough activation and proliferation despite CoBS treatment. Thus, although most T-cell subpopulations remained quiescent during CoBS treatment, the $CD28^-$ $CD8^+$ T-cell subpopulation showed breakthrough activation (loss of BCl-2) and proliferation (gain of Ki-67). The isolated activation of the $CD28^-$ $CD8^+$ T-cell cohort is especially notable, given that CoBS immunosuppression includes CD28-blockade with CTLA4Ig. $CD28^-$ cells effectively receive less immunosuppression under this regimen and thus may be at greater risk for breakthrough alloactivation. There is precedent for this hypothesis from a primate renal transplant model: Weaver et al[23] have shown that, although costimulation blockade–resistant rejection occurred with CTLA4Ig, the addition of alefacept, an agent able to target $CD28^-$ cells, led to significant prolongation of allograft survival. These results suggest that the addition of alefacept may also improve GVHD control when added to a CTLA4Ig-based prophylaxis strategy. Future studies with this model will allow this hypothesis to be tested directly.

It is important to note that, although CoBS may have been inadequate to fully prevent GVHD in this high-risk T cell–replete model of haploidentical transplantation, it may show improved efficacy at controlling the alloresponse during targeted T-cell add-back after T cell–depleted haploidentical BMT. Thus, the last decade has witnessed significant advances in T cell–depleted haploidentical BMT, including recent progress with targeted add-back of allo-depleted T cells.[24,51-55] In these clinical scenarios, the reduced numbers of transferred T cells might be more effectively controlled with combined sirolimus/costimulation blockade, leading to more complete clinical efficacy than observed in our T cell–replete transplantation model.

Although the results presented here suggest that the reservoir of CoBS-resistant alloreactivity ultimately resided in the $CD28^-/CD95^+$ subpopulation (Figure 6D,F) and that in vitro CTLA4Ig was effective in inhibiting alloproliferation of both $CD28^+CD95^-$ naive cells and $CD28^+/CD95^+$ effectors (Figure 6E), they do not rule out that in vivo CoBS may fail to fully prevent the alloactivation of $CD28^+$ naive T cells and their subsequent conversion to $CD28^-$ effector cells. This hypothesis can best be tested by transferring purified naive T cells or purified $CD28^-/CD95^+$ effector cells into recipients and by determining the relative efficacy of CoBS to inhibit GVHD arising from the transferred cells. This represents an important area for future investigation, in which the MHC-defined primate model of GVHD will be able to facilitate rigorous preclinical testing of the relative propensities of purified T-cell populations to cause GVHD.

## Acknowledgments

We thank Rainer Storb for his advice and input regarding the establishment of the primate GVHD model, and also thank Daniel Promislow for statistical analysis.

This work was supported by Yerkes National Primate Research Center (base grant RR00165); by the National Institutes of Health (grants 2U19 AI051731 and 2P01 AI044644, C.P.L.; grants 5K08 AI065822, 2U19 AI051731, 1 R01 HL095791-01A1, and 2U24 RR018109, L.S.K.; grant U24 RR18144-01, M.C.T.P. and T.W.; grants NIH 2R01 HL56067, RO1 AI 34495, R01 HL 63452, and P01 AI 056299, B.R.B.); and

**Figure 5. The effect of CoBS immunosuppression on GVHD.** (A) Lymphocyte proliferation was inhibited in animals treated with CoBS. Representative example of R.5 showing forward-scatter versus side-scatter characteristics before transplantation (top) and on day 43 (bottom), during CoBS treatment. (B) Longitudinal analysis of the white blood cell (WBC) count, absolute neutrophil count (ANC) and absolute lymphocyte count (ALC) in R.4-R.7. (C) Survival advantage observed with CoBS immunosuppression. At the 30-day primary endpoint, all untreated animals had died, and 100% of CoBS-treated animals survived ($P = .01$). (D) Extended survival analysis of CoBS-treated versus untreated cohorts. Log-rank analysis indicated that overall survival of the CoBS-treated cohort (MST = 62 days) was statistically significantly different from the untreated cohort (MST = 11.6 days; $P = .01$). MST = mean survival time. (E) Photomicrographs of hematoxylin and eosin staining of the lungs, liver, and colon of the autologous transplant control (R.10), a representative CoBS-treated recipient who developed significant breakthrough GVHD (R.4), and a representative CoBS-treated recipient who showed minimal GVHD histopathology (R.5). Bar = 100 μm. These studies used an Olympus BX51 microscope (Olympus America), using a 10×/0.40 UPlan Apo lens (Olympus). Slides were mounted with Permount solution (Sigma-Aldrich) and photographs were taken with the Spot RT Slider imaging system (Spot Imaging Solutions). Image analysis was performed using Spot Advanced Version 4.6 (Spot Imaging Solutions), and image processing was performed using Photoshop CS4 extended v11.01 (Adobe). (F) Correlation of clinical disability (as measured by the activity score) with GVHD histopathology. The data fit a linear equation with an $R^2 = 0.7221$. (G) Longitudinal analysis of weight loss in animals treated with CoBS immunosuppression.

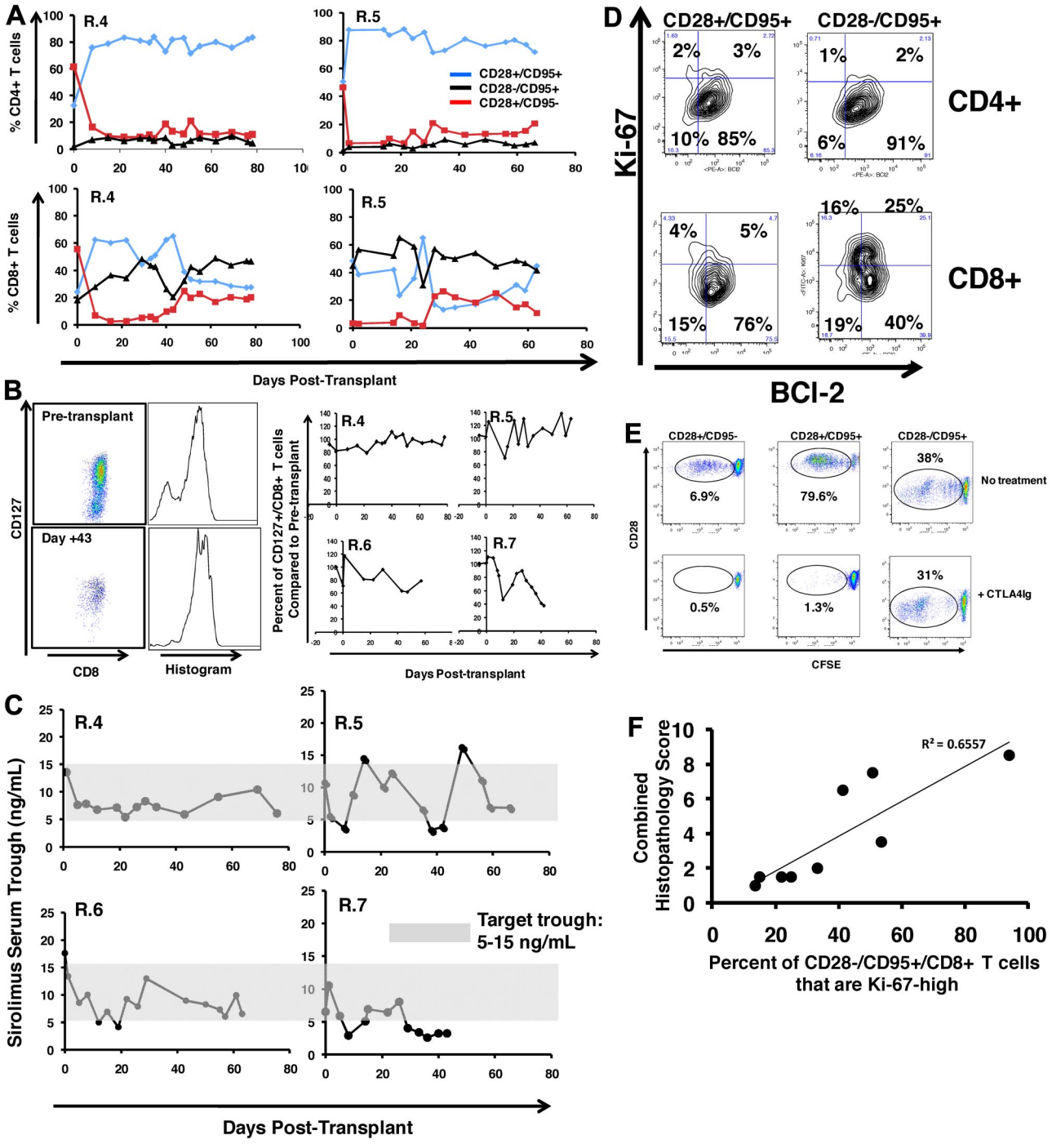


**Figure 6. Flow cytometric analysis of CoBS-treated transplant recipients.** (A) Longitudinal analysis of representative $CD4^+$ (top) and $CD8^+$ (bottom) T-cell subsets during CoBS treatment (R.4 and R.5 are shown). (B) CD127 expression on $CD8^+$ T cells in CoBS-treated animals. (Left) Pseudocolor dot plots and histogram analysis are representative of CD127 expression on $CD8^+$ T cells from R.5 analyzed both before transplantation (top) and on day 43 after transplantation (bottom). (Right) Longitudinal analysis is shown of CD127 expression on $CD8^+$ T cells in R.4-R.7 normalized for pretransplantation expression levels of CD127. (C) Sirolimus levels measured longitudinally in animals R.4-R.7. The shaded area is the target trough range: 5-15 ng/mL. (D) BCl-2 and Ki-67 on $CD4^+$ and $CD8^+$ $CD28^+/CD95^+$ and $CD28^-/CD95^+$ T cells in a representative CoBS-treated animal (R.4). (E) CTLA4Ig-resistant alloproliferation of $CD28^-$ T cells as measured by CFSE (5,6-carboxyfluorescein diacetate, succinimidyl ester) MLR. (Top) Representative dot plots showing T-cell alloproliferation in $CD28^+/CD95^-$, $CD28^+/CD95^+$, and $CD28^-/CD95^+$ T-cell populations in the absence of CTA4Ig treatment. (Bottom) Representative dot plots showing T-cell alloproliferation in $CD28^+/CD95^-$, $CD28^+/CD95^+$, and CD28-$^-CD95^+$ T-cell populations in the presence of 1.6μM CTLA4Ig, showing CTLA4Ig-resistant alloproliferation existing in the $CD28^-/CD95^+$ subpopulation. A dose-response curve of 0.8-12.8μM CTLA4Ig was performed (not shown), with similar results observed for all concentrations of CTLA4Ig tested. For each population, the percentage of cells that had undergone ≥ 1 cell division was measured with FlowJo flow cytometry analysis software (Tree Star) and is noted on the corresponding dot plots. (F) Correlation of the percentage of Ki-$67^{high}$ $CD28^-/CD95^+$ $CD8^+$ T cells with GVHD histopathology scores. The maximal percentage of $CD28^-/CD95^+/CD8^+$ cells that up-regulated Ki-67 was compared with the total histopathology score (Table 4). The data fit a linear equation with an $R^2 = 0.6557$.

by a Burroughs Wellcome Fund Career Award in the Biomedical Sciences (L.S.K.). L.S.K. and C.P.L. are members of the Children's Healthcare of Atlanta Transplant Immunology and Immune Therapeutics Center.

## Authorship

Contribution: W.P.M. designed and performed research and analyzed data; S. Srinivasan, A.P.-M., L.S., J.B., D.C.A., P.S., A.G., and I.C. performed research and analyzed data; K.S., S. Sen, K.H., T.D., A.T., C.W., E.S., E.E., T.C., M.C.T.P., T.W., and M.S. performed research; J.H. designed research and interpreted data; C.P.L. designed research and analyzed data; B.R.B. analyzed data and wrote the paper; L.S.K. designed and performed research, analyzed data, and wrote the paper.

Conflict-of-interest disclosure: The authors declare no competing financial interests.

The current affiliation for W.P.M. is Department of Pediatric Hematology-Oncology, University of Minnesota, Minneapolis, MN.

Correspondence: Leslie S. Kean, Department of Pediatrics, Emory University School of Medicine, Rm 5203 WMB, 101 Woodruff Cir NE, Atlanta, GA 30322; e-mail: Leslie.Kean@emory.edu.

## References

1. Cruzado JM, Bestard O, Grinyo JM. New immunosuppressive protocols with the advent of novel biological drugs. *Transplantation.* 2009;88(3 suppl):S20-S23.
2. Adams AB, Durham MM, Kean L, et al. Costimulation blockade, busulfan, and bone marrow promote titratable macrochimerism, induce transplantation tolerance, and correct genetic hemoglobinopathies with minimal myelosuppression. *J Immunol.* 2001;167(2):1103-1111.
3. Aoyagi T, Yamashita K, Suzuki T, et al. A human anti-CD40 monoclonal antibody, 4D11, for kidney transplantation in cynomolgus monkeys: induction and maintenance therapy. *Am J Transplant.* 2009;9(8):1732-1741.
4. Bluestone JA, St Clair EW, Turka LA. CTLA4Ig: bridging the basic immunology with clinical application. *Immunity.* 2006;24(3):233-238.
5. Gilson CR, Milas Z, Gangappa S, et al. Anti-CD40 monoclonal antibody synergizes with CTLA4Ig in promoting long-term graft survival in murine models of transplantation. *J Immunol.* 2009;183(3):1625-1635.
6. Linsley PS, Nadler SG. The clinical utility of inhibiting CD28-mediated costimulation. *Immunol Rev.* 2009;229(1):307-321.
7. Vincenti F. Costimulation blockade in autoimmunity and transplantation. *J Allergy Clin Immunol.* 2008;121(2):299-306; quiz 7-8.
8. Vincenti F, Charpentier B, Vanrenterghem Y, et al. A phase III study of belatacept-based immunosuppression regimens versus cyclosporine in renal transplant recipients (BENEFIT study). *Am J Transplant.* 2010;10(3):535-546.
9. Durham MM, Bingaman AW, Adams AB, et al. Cutting edge: administration of anti-CD40 ligand and donor bone marrow leads to hemopoietic chimerism and donor-specific tolerance without cytoreductive conditioning. *J Immunol.* 2000;165(1):1-4.
10. Fehr T, Takeuchi Y, Kurtz J, Wekerle T, Sykes M. Early regulation of CD8 T cell alloreactivity by CD4+CD25- T cells in recipients of anti-CD154 antibody and allogeneic BMT is followed by rapid peripheral deletion of donor-reactive CD8+ T cells, precluding a role for sustained regulation. *Eur J Immunol.* 2005;35(9):2679-2690.
11. Ito H, Takeuchi Y, Shaffer J, Sykes M. Anti-CD40L monoclonal antibodies can replace anti-CD4 monoclonal antibodies for the nonmyeloablative induction of mixed xenogeneic chimerism. *Transplantation.* 2006;82(2):251-257.
12. Larsen CP, Alexander DZ, Hollenbaugh D, et al. CD40-gp39 interactions play a critical role during allograft rejection. Suppression of allograft rejection by blockade of the CD40-gp39 pathway. *Transplantation.* 1996;61(1):4-9.
13. Larsen CP, Elwood ET, Alexander DZ, et al. Long-term acceptance of skin and cardiac allografts after blocking CD40 and CD28 pathways. *Nature.* 1996;381(6581):434-438.
14. Rigby MR, Trexler AM, Pearson TC, Larsen CP. CD28/CD154 blockade prevents autoimmune diabetes by inducing nondeletional tolerance after effector t-cell inhibition and regulatory T-cell expansion. *Diabetes.* 2008;57(10):2672-2683.
15. Li XL, Menoret S, Le Mauff B, Angin M, Anegon I. Promises and obstacles for the blockade of CD40-CD40L interactions in allotransplantation. *Transplantation.* 2008;86(1):10-15.
16. Imai A, Suzuki T, Sugitani A, et al. A novel fully human anti-CD40 monoclonal antibody, 4D11, for kidney transplantation in cynomolgus monkeys. *Transplantation.* 2007;84(8):1020-1028.
17. Pearson TC, Trambley J, Odom K, et al. Anti-CD40 therapy extends renal allograft survival in rhesus macaques. *Transplantation.* 2002;74(7):933-940.
18. Li Y, Li XC, Zheng XX, Wells AD, Turka LA, Strom TB. Blocking both signal 1 and signal 2 of T-cell activation prevents apoptosis of alloreactive T cells and induction of peripheral allograft tolerance. *Nat Med.* 1999;5(11):1298-1302.
19. Smiley ST, Csizmadia V, Gao W, Turka LA, Hancock WW. Differential effects of cyclosporine A, methylprednisolone, mycophenolate, and rapamycin on CD154 induction and requirement for NFkappaB: implications for tolerance induction. *Transplantation.* 2000;70(3):415-419.
20. Wells AD, Li XC, Li Y, et al. Requirement for T-cell apoptosis in the induction of peripheral transplantation tolerance. *Nat Med.* 1999;5(11):1303-1307.
21. Adams AB, Williams MA, Jones TR, et al. Heterologous immunity provides a potent barrier to transplantation tolerance. *J Clin Invest.* 2003;111(12):1887-1895.
22. Kean LS, Adams AB, Strobert E, et al. Induction of chimerism in rhesus macaques through stem cell transplant and costimulation blockade-based immunosuppression. *Am J Transplant.* 2007;7(2):320-335.
23. Weaver TA, Charafeddine AH, Agarwal A, et al. Alefacept promotes co-stimulation blockade based allograft survival in nonhuman primates. *Nat Med.* 2009;15(7):746-749.
24. Davies JK, Gribben JG, Brennan LL, Yuk D, Nadler LM, Guinan EC. Outcome of alloanergized haploidentical bone marrow transplantation after ex vivo costimulatory blockade: results of 2 phase 1 studies. *Blood.* 2008;112(6):2232-2241.
25. Blazar BR, Taylor PA, Linsley PS, Vallera DA. In vivo blockade of CD28/CTLA4: B7/BB1 interaction with CTLA4Ig reduces lethal murine graft-versus-host disease across the major histocompatibility complex barrier in mice. *Blood.* 1994;83(12):3815-3825.
26. Ohata J, Sakurai J, Saito K, Tani K, Asano S, Azuma M. Differential graft-versus-leukaemia effect by CD28 and CD40 co-stimulatory blockade after graft-versus-host disease prophylaxis. *Clin Exp Immunol.* 2002;129(1):61-68.
27. Tamada K, Tamura H, Flies D, et al. Blockade of LIGHT/LTbeta and CD40 signaling induces allospecific T cell anergy, preventing graft-versus-host disease. *J Clin Invest.* 2002;109(4):549-557.
28. Taylor PA, Friedman TM, Korngold R, Noelle RJ, Blazar BR. Tolerance induction of alloreactive T cells via ex vivo blockade of the CD40:CD40L costimulatory pathway results in the generation of a potent immune regulatory cell. *Blood.* 2002;99(12):4601-4609.
29. Via CS, Rus V, Nguyen P, Linsley P, Gause WC. Differential effect of CTLA4Ig on murine graft-versus-host disease (GVHD) development: CTLA4Ig prevents both acute and chronic GVHD development but reverses only chronic GVHD. *J Immunol.* 1996;157(9):4258-4267.
30. Yu C, Linsley P, Seidel K, Sale G, Deeg HJ, Nash RA, et al. Cytotoxic T lymphocyte antigen 4-immunoglobulin fusion protein combined with methotrexate/cyclosporine as graft-versus-host disease prevention in a canine dog leukocyte antigen-nonidentical marrow transplant model. *Transplantation.* 2000;69(3):450-454.
31. Penedo MC, Bontrop RE, Heijmans CM, et al. Microsatellite typing of the rhesus macaque MHC region. *Immunogenetics.* 2005;57(3-4):198-209.
32. Blazar BR, Taylor PA, McElmurry R, et al. Engraftment of severe combined immune deficient mice receiving allogeneic bone marrow via in utero or postnatal transfer. *Blood.* 1998;92(10):3949-3959.
33. Woodruff JM, Eltringham JR, Casey HW. Early secondary disease in the Rhesus monkey, I: a comparative histopathologic study. *Lab Invest.* 1969;20(6):499-511.
34. Benito JM, Lopez M, Lozano S, Gonzalez-Lahoz J, Soriano V. Down-regulation of interleukin-7 receptor (CD127) in HIV infection is associated with T cell activation and is a main factor influencing restoration of CD4(+) cells after antiretroviral therapy. *J Infect Dis.* 2008;198(10):1466-1473.
35. Faller E, Kakal J, Kumar R, Macpherson P. IL-7 and the HIV Tat protein act synergistically to down-regulate CD127 expression on CD8 T cells. *Int Immunol.* 2009;21(3):203-316.
36. Alpdogan O, Muriglan SJ, Eng JM, et al. IL-7 enhances peripheral T cell reconstitution after allogeneic hematopoietic stem cell transplantation. *J Clin Invest.* 2003;112(7):1095-1107.
37. Pitcher CJ, Hagen SI, Walker JM, et al. Development and homeostasis of T cell memory in rhesus macaque. *J Immunol.* 2002;168(1):29-43.
38. Shlomchik WD. Graft-versus-host disease. *Nat Rev Immunol.* 2007;7(5):340-352.
39. Dereuddre-Bosquet N, Vaslin B, Delache B, t al. Rapid modifications of peripheral T-cell subsets that express CD127 in macaques treated with recombinant IL-7. *J Med Primatol.* 2007;36(4-5):228-237.
40. Doisne JM, Urrutia A, Lacabaratz-Porret C, et al. CD8+ T cells specific for EBV, cytomegalovirus, and influenza virus are activated during primary HIV infection. *J Immunol.* 2004;173(4):2410-2418.
41. Zaunders JJ, Munier ML, Kaufmann DE, et al. Early proliferation of CCR5(+) CD38(+++) antigen-specific CD4(+) Th1 effector cells during primary HIV-1 infection. *Blood.* 2005;106(5):1660-1667.
42. Shedlock DJ, Talbott KT, Morrow MP, et al. Ki-67 staining for determination of rhesus macaque T cell proliferative responses ex vivo. *Cytometry A.* 2010;77(3):275-284.

43. Kmieciak M, Gowda M, Graham L, et al. Human T cells express CD25 and Foxp3 upon activation and exhibit effector/memory phenotypes without any regulatory/suppressor function. *J Transl Med.* 2009;7:89.

44. Anderson A, Martens CL, Hendrix R, et al. Expanded nonhuman primate tregs exhibit a unique gene expression signature and potently downregulate alloimmune responses. *Am J Transplant.* 2008;8(11):2252-2264.

45. Paczesny S, Krijanovski OI, Braun TM, et al. A biomarker panel for acute graft-versus-host disease. *Blood.* 2009;113(2):273-278.

46. Carlson MJ, West ML, Coghill JM, Panoskaltsis-Mortari A, Blazar BR, Serody JS. In vitro-differentiated TH17 cells mediate lethal acute graft-versus-host disease with severe cutaneous and pulmonary pathologic manifestations. *Blood.* 2009;113(6):1365-1374.

47. Yi T, Chen Y, Wang L, et al. Reciprocal differentiation and tissue-specific pathogenesis of Th1, Th2, and Th17 cells in graft-versus-host disease. *Blood.* 2009;114(14):3101-3112.

48. Ream RM, Sun J, Braciale TJ. Stimulation of naive CD8+ T cells by a variant viral epitope induces activation and enhanced apoptosis. *J Immunol.* 2010;184(5):2401-2409.

49. Sandau MM, Kohlmeier JE, Woodland DL, Jameson SC. IL-15 regulates both quantitative and qualitative features of the memory CD8 T cell pool. *J Immunol.* 2010;184(1):35-44.

50. Lin MT, Tseng LH, Frangoul H, et al. Increased apoptosis of peripheral blood T cells following allogeneic hematopoietic cell transplantation. *Blood.* 2000;95(12):3832-3839.

51. Aversa F, Reisner Y, Martelli MF. The haploidentical option for high-risk haematological malignancies. *Blood Cells Mol Dis.* 2008;40(1):8-12.

52. Aversa F, Tabilio A, Velardi A, et al. Treatment of high-risk acute leukemia with T-cell-depleted stem cells from related donors with one fully mismatched HLA haplotype. *N Engl J Med.* 1998; 339(17):1186-1193.

53. Aversa F, Terenzi A, Tabilio A, et al. Full haplotype-mismatched hematopoietic stem-cell transplantation: a phase II study in patients with acute leukemia at high risk of relapse. *J Clin Oncol.* 2005;23(15):3447-3454.

54. Guinan EC, Boussiotis VA, Neuberg D, et al. Transplantation of anergic histoincompatible bone marrow allografts. *N Engl J Med.* 1999; 340(22):1704-1714.

55. Hagin D, Reisner Y. Haploidentical bone marrow transplantation in primary immune deficiency: stem cell selection and manipulation. *Immunol Allergy Clin North Am.* 2010;30(1):45-62.